

University of Nebraska - Lincoln

DigitalCommons@University of Nebraska - Lincoln

Environmental Engineering Theses and Graduate
Student Research

Environmental Engineering Program

5-2019

Theoretical Model for Shields Diagram and Its Application

Jichao Jiang

University of Nebraska-Lincoln, 282856940@qq.com

Follow this and additional works at: <https://digitalcommons.unl.edu/envengdiss>

Part of the [Environmental Engineering Commons](#)

Jiang, Jichao, "Theoretical Model for Shields Diagram and Its Application" (2019). *Environmental Engineering Theses and Graduate Student Research*. 18.

<https://digitalcommons.unl.edu/envengdiss/18>

This Article is brought to you for free and open access by the Environmental Engineering Program at DigitalCommons@University of Nebraska - Lincoln. It has been accepted for inclusion in Environmental Engineering Theses and Graduate Student Research by an authorized administrator of DigitalCommons@University of Nebraska - Lincoln.

THEORETICAL MODEL FOR SHIELDS DIAGRAM AND ITS
APPLICATION

By

Jichao Jiang

A THESIS

Presented to the Faculty of

The Graduate College at The University of Nebraska

In Partial Fulfillment of Requirements

For the Degree of Master of Science

Major: Environmental Engineering

Under the Supervision of Professor Junke.Guo

Lincoln, Nebraska

May, 2019

—

THEORETICAL MODEL FOR SHIELDS DIAGRAM AND ITS
APPLICATION

Jichao Jiang, M.S

University of Nebraska, 2019

Advisor: Junke.Guo

The transition from the condition of “no motion” to initial sediment moment, defined as sediment initiation, has been related to practical engineering (channel degradation, stable channel design), oceanographic (dredging, pipelines, cables), sedimentologic (sediment mobility, transport rates), geologic (the hydraulic interpretation of paleoenvironments), geochemical (pollutant transport), and gained considerable interest since nineteenth century.

Shields diagram for sediment initiation in terms of critical shear stress is a classic problem in sediment transport, but it is still an empirical law without a simple and practical theory despite extensive research since the 1930s. Hence, this research presents a simple theoretical model for critical shear stress, which has four lumped parameters determined analytically and fits data from various references in the Shields diagram. Specifically, it first describes the hydrodynamic drag on a bed particle with Forchheimer's law from porous media flow; it then models the cohesive force between sediment particles by considering the effects of attached water film and electrostatics. The resulting dimensionless critical shear stress (or the critical Shields parameter) is a rational function of particle Reynolds number, which reproduces the Shields diagram by tending to two constants for small and large particle Reynolds

numbers, respectively, and having a minimum value in the transitional regime. For applications, the proposed rational function can be solved for a critical shear stress or a critical sediment size analytically without numerical iterations.

Keywords: Bedload; critical shear stress; incipient motion; sediment threshold; sediment transport; Shields diagram; Shields parameter

ACKNOWLEDGEMENTS

This work is not an absolutely personal effort of me. It is impossible to finish without help of many people along the way. I would appreciate every person who contributed to it, was patient with me in the past two years, and encouraged me to finish this huge thesis.

First and foremost, I'd like to thank to my academic advisor Dr. Junke Guo for his leadership, patience, and teaching over last several years of graduate school. I really appreciate the countless personal meetings and discussions. I have learned more than I ever expected to, thanks him to teach me how to finish a tough work like this and show the example of the way he worked and succeed. Additionally, thanks go to Dr. Bruce Dvorak for his guidance and giving me opportunities to present my thesis in the Civil Engineering Seminar that allowed me to introduce my work to my classmates and professional researchers.

I want to show my sincere gratitude to my family for their incredible love and support, and the time they spent with me. Those people, who always wish good to me, expect and push me to be a better person no matter where I am and what I do.

I also want to thank my undergraduate advisor Dr. Christian Binek and Dr. Bob Kelty, who showed me beautiful and attractive science world and taught me always hunger for knowledge no matter what I have achieved.

Lastly, I thank all friends, classmates, colleagues and teachers in the University of Nebraska. The time I spent over eight years in Lincoln are enjoyable and memorable.

TABLE OF CONTENTS

TABLE OF CONTENTS	ii
LIST OF FIGURES.....	iv
LIST OF ABBREVIATIONS	v
Chapter 1 Introduction.....	1
1.1 Background.....	1
1.2 Research objective	1
1.3 Thesis Organization.....	2
Chapter 2 Literature review on experimental facts.....	3
2.1 Introduction	3
2.2 Mathematical Modeling of Critical Shear Stress.....	3
2.3 Summary.....	7
Chapter 3 Evaluation of Factors of Sediment incipient Motion.....	9
3.1 Introduction Definition of Sediment Incipient Motion	9
3.2 Hydrodynamic Force.....	11
3.3 Cohesive Force	12
3.4 Critical Shear Stress.....	17
Chapter 4 Application	19
4.2 Critical shear stress for sediment transport	19
4.3 Riprap design of channel bed.....	22
Chapter 5 Conclusion and Recommendations.....	24

5.1 Conclusion.....	25
5.2 Significance of model	26
5.3 Recommendation for future work.....	27
References.....	28
Appendix I. Generalization of Shields Diagram	32

LIST OF FIGURES

Figure 2.1: Shields Diagram for Sediment Initiation	5
Figure 2.2: Extended Shields diagram by Mants and Yalin and Karahan.....	7
Figure 3.1: River flow with (a) velocity profile over a within porous bed.....	10
Figure 3.1: River flow with (b) forces on a bed particle.....	10
Figure 3.2: Cohesion between two sediment particles: (a) in water.....	13
Figure 3.2: Cohesion between two sediment particles: (b) in air.....	13
Figure 4.1: Graphical interpretation for solution.....	20
Figure 4.2: Explicit Shields diagram in terms of $\tau_{*c} = f(D^*)$	21
Figure 5.1: Generalization of Shields diagram.....	23

LIST OF ABBREVIATIONS

The following symbols are used in this thesis:

A, B, C, E	=	lumped model parameters (-)
A_c	=	contact area (m^2)
C_d	=	drag coefficient (-)
D, D_1, D_2	=	sediment diameters (m)
D^*	=	dimensionless sediment diameter (-)
F_c	=	cohesive force (N)
F_d	=	hydrodynamic drag (N)
F_f	=	friction (N)
F_l	=	hydrodynamic lift (N)
F_n	=	normal force (N)
f	=	functional symbol (-)
g	=	gravity acceleration (ms^{-2})
h	=	flow depth (m)
M, N	=	interim parameters (-)
m	=	model parameter (-)
p, q	=	interim parameters (-)
q_b	=	unit volumetric bedload transport rate (m^2s^{-1})
R^*	=	Reynolds number (-)
R_c	=	critical particle Reynolds number (-)

$R_{c \min}$	=	critical particle Reynolds number at minimum τ^*_{*c} (-)
S_0	=	channel bottom slope (-)
t	=	distance between surfaces of two particles (m)
$u(y)$	=	velocity distribution (ms^{-1})
u^*_{*c}	=	critical shear velocity (ms^{-2})
V	=	bulk velocity through first layer bed particles (ms^{-1})
W	=	submerged sediment particle weight (N)
x	=	dimensionless parameter of critical shear stress (-)
y	=	distance from channel bed (m)
α, β	=	model parameters (-)
γ	=	specific weight of water (kgm^{-3})
γ_s	=	specific weight of sediment (kgm^{-3})
Δ	=	γ_s / γ specific gravity of sediment (-)
Δ_0, Δ_1	=	interim parameters (-)
δ	=	thickness of attached water on sediment surface (m)
λ	=	interim parameter (-)
ν	=	kinematic water viscosity (m^2s^{-1})
ρ	=	water density (kg m^{-3})
ρ_s	=	sediment density (kg m^{-3})
τ_s	=	critical shear stress (Pa)
τ_0	=	shear stress applied on bed sediment (Pa)
τ^*_{*c}	=	dimensionless critical shear stress or critical Shields parameter (-)

- $\tau_{*c \min}$ = minimum dimensionless critical shear stress or critical Shields parameter (-)
- τ_{*c0} = left limit dimensionless critical shear stress or critical Shields parameter (-)
- $\tau_{*c\infty}$ = right limit dimensionless critical shear stress or critical Shields parameter (-)
- Φ = sediment repose angle (-)

CHAPTER 1

INTRODUCTION

1.1 Background

Shields diagram is a fundamental law in sediment transport, describing the critical shear stress under sediment incipient (or threshold) condition (Chien and Wan 1999; Garcia 2008; Julien 2010; Jan 2018). It is widely used in river and coastal engineering in selecting sediment size, estimating scour depth, and predicting bedload transport (Fredsoe and Deigaard 1992; Roarty and Bruno 2006, She et al. 2014); it is also applied in design of sewer and drainage systems in municipal engineering. Nevertheless, it is still an empirical law expressed by many empirical functions (Dey 2014) without a simple and practical theory despite extensive research (Buffington and Montgomery 1997) since Shields (1936), because of the complicated flow at the water-bed interface.

1.2 Research objective

This research intends to propose a theoretical model for sediment initiation, which can reproduce the empirical curve in the extended Shields diagram (Mants 1977; Yalin and Karahan 1979; Julien 2010) and help us achieve a deeper understanding of the nature of incipient motion of sediment transport and prediction

methods. To this end, it starts with a literature review on experimental facts that make a foundation for this research; it then sequentially discusses the definitions of sediment initiation, hydrodynamic drag, cohesive force, and critical shear stress. It also demonstrates applications of the theoretical model in solving for critical shear stress in sediment transport and for sediment diameter in river and coastal engineering.

1.3 Thesis Organization

This thesis is organized into five chapters. Chapter 2 provides a brief review of relevant literature sources, focusing on the critical shear stress method, and shields diagram. Sediment initiation fundamentals and characteristics of shields diagram are discussed here. Chapter 3 describes the conditions of sediment incipient motion studied in this research, along with the key assumptions and limitations. Three factors- hydrodynamic force, cohesive force, and critical shear stress are defined in details in chapter 3. Chapter 4 contains the applications of critical shear stress for sediment transport and stable channel design of channel bed. Chapter 5 includes a brief summary of the theoretical model for the shields diagrams. Finally, the appendices present detailed steps for generalization of shields diagram and graphical analysis.

CHAPTER 2

LITERATURE REVIEW ON EXPERIMENTAL FACTS

2.1 Introduction

Sediment initiation was extensively studied in literature in terms of a critical velocity (Xie 1980; Han and He 1999) and a critical shear stress (Buffington 1999). The critical velocity method correlates sediment initiation to an average flow velocity by a resistance law, whereas the critical shear stress method correlates the initiation to a bed shear stress. Both methods are still far from complete because of poor understanding of the water-sediment interactions (drag and lift) and sediment-sediment interactions (adhesion and cohesion) at the bed.

In the context of this research, the following review is limited to the shear stress method, highlighting the experimental data, which are fundamental in the development of the Shields diagram.

2.2 Mathematical Modeling of Critical Shear Stress

First, the concept of the critical shear stress τ_c was introduced by Du Boys (1879) who expressed unit bedload transport rate q_b as (Hager 2005):

$$q_b \propto \tau_o (\tau_o - \tau_c) \quad (2.1)$$

where τ_o is shear stress applied on bed sediment, and $\tau_o - \tau_c$ is called the excess shear stress. Eq. (2.1) states that sediment starts to move only if $\tau_o \geq \tau_c$. Since Du Boys (1879), the excess shear stress, $\tau_o - \tau_c$, has been used in many of bedload transport formulas (Chien and Wan 1999). Therefore, the determination of the critical shear stress τ_c is necessary in predicting sediment transport.

Shields (1936) pioneered the study of quantifying τ_c by applying similarity principles and turbulent boundary layer theory to bedload transport (Rouse 1939; Kennedy 1995; Buffington 1999; Guo 2002). Because the flow at the water-bed interface is very complicated, it is very difficult to unify laminar and turbulent flows, including velocity distributions and friction factors, into a simple single equation (even today). Hence, Shields could not formulate a specific function for sediment initiation; he expressed his results only in a similarity law:

$$\frac{\tau_c}{(\gamma_s - \gamma)D} = f\left(\frac{u_{*c}D}{\nu}\right) \quad (2.2)$$

Where γ_s = specific weight of sediment, γ = specific weight of water, D = diameter of sediment, ν =kinematic water viscosity, and $u_{*c} = \sqrt{\tau_c/\rho}$ is the critical shear velocity with ρ =water density. The left-hand side of Eq. (2.2) is called the dimensionless critical shear stress or the critical Shields parameter, denoted as

$$\tau_{*c} = \frac{\tau_c}{(\gamma_s - \gamma)D} \quad (2.3)$$

which expresses the ratio of the hydrodynamic force to the resistance due to gravity.

The right-hand side of Eq. (2.2) states that the critical Shields parameter τ_{*c} is a function of the particle Reynolds number, denoted as $R_{*c} = \frac{u_{*c}D}{\nu}$, which represents

the ratio of the sediment diameter D to the viscous thickness $\frac{\nu}{u_{*c}}$. Eq. (2.2) then becomes

$$\tau_{*c} = f(R_{*c}) \quad (2.4)$$

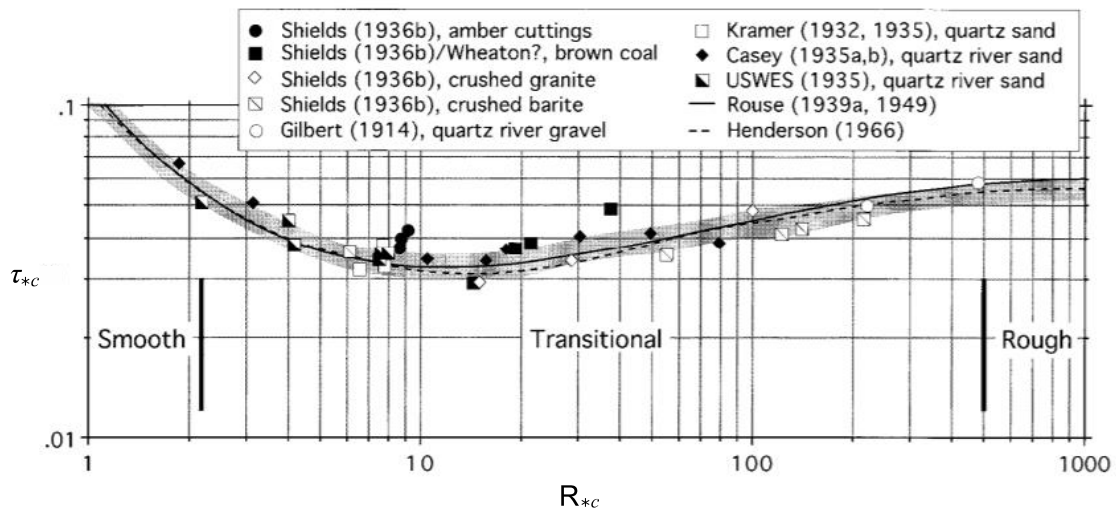


Figure 2.1: Shields Diagram for Sediment Initiation [adopted from Buffington (1999)]

Shields determined this functional relationship experimentally. He did a series of experiments with different particle diameters, specific weights and flow conditions. He then plotted his data according to Eq. (2.4), together with those from references, in Fig. 2.1, which is now called the Shields diagram.

By analogy to the effect of roughness on turbulent boundary layer flow, Shields divided Fig. 2.1 into three regimes: smooth ($R_{*c} \leq 2$), transitional ($2 \leq R_{*c} \leq 500$), and turbulent ($R_{*c} \geq 500$). In the smooth regime, sediment is completely embedded in viscous sublayer, Shield analytically predicted

$$\tau_{*c} = \frac{0.1}{R_{*c}} \quad (2.5)$$

which implies that the dimensional value of τ_c is independent of D (Shields 1936; Chien and Wan 1999). Yet, he did not have enough data in this regime. In the rough turbulent regime, the flow is independent of viscosity; Shields concluded that τ_{*c} must tend to a constant of 0.06 (this research takes it as 0.055 below). In the transitional turbulent regime, τ_c has a minimum value 0.033 at $R_{*c} \simeq 10$ (this research takes it as 14 below) , meaning that when sediment diameter D is approximately the viscous sublayer thickness $11.6\nu/u_{*c}$, sediment starts to move easily.

Mants (1977) extended the Shields diagram by adding experimental data in the laminar regime ($R_{*c} \leq 2$). He found that the measured data in this regime are significantly less than those predicted by Eq. (2.5), and τ_c in this regime does depend on D . Yalin and Karahan (1979) enriched the data in the smooth turbulent flow regime, and confirmed Mants' findings. They further compiled data from many sources in Fig. 2.2, which is often called the extended Shields diagram, which shows three characteristics:

(1) For smaller R_{*c} , τ_{*c} tends to a constant of 0.25, meaning

$$\tau_{*c}(R_{*c} \rightarrow 0) \simeq 1/4 \quad (2.6)$$

(2) For very large R_{*c} , τ_{*c} tends to a constant of 0.056, meaning

$$\tau_{*c}(R_{*c} \rightarrow \infty) \simeq 1/18 \quad (2.7)$$

(3) At $R_{*c} \simeq 14$, τ_{*c} reaches a minimum value of 0.033, meaning

$$\tau_{*c}(R_{*c} \simeq 14) \simeq 1/30 \quad (2.8)$$

$$\frac{d\tau_{*c}}{dR_{*c}}(R_{*c} \simeq 14) = 0 \quad (2.9)$$

Eqs. (2.6)-(2.9) are restrictions for establishing any empirical or theoretical model for sediment initiation.

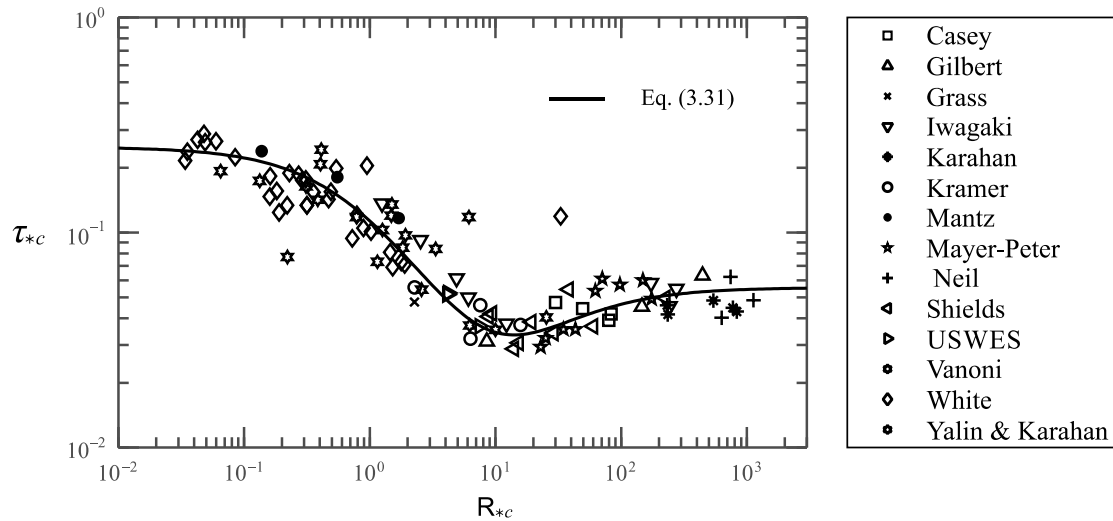


Figure 2.2: Extended Shields diagram by Mantz (1977) and Yalin and Karahan

2.3 Summary

Many empirical functions and theoretical formulations have been proposed for Eq. (2.4) in the literature (Buffington and Montgomery 1997; Cheng and Chiew 1999; Armanini 2005; Cao et al. 2006; She et al. 2006; Lamb et al. 2008; Miedema 2010; Julien 2010; Bravo et al. 2014; Simoes 2014; Roušar et al. 2016). Empirical functions, though convenient in applications, lack physical meanings, while theoretical formulations are still limited by turbulence knowledge at the water-bed interface because the modeling of roughness effects on turbulent flow (Nikuradse diagram for friction factor) does not change much since Shields (1936). Particularly, most of theoretical formulations assumed that (1) sediment is cohesionless, and (2) a turbulent

boundary layer velocity distribution law can be extended into the porous bed (at least near the bed surface), which is then used to model the hydrodynamic drag and lift on a sediment particle. No matter how good or bad these assumptions are, the resulting Shields diagram seldom meets all of the restrictions defined by Eqs. (2.6)-(2.9). Furthermore, the results are often too complicated to apply in practice.

In what follows, this research presents a theoretical model that is physically based on the porous bed flow instead of the channel boundary layer flow, mathematically meets Eqs. (2.6)-(2.9) and fits the data in the Shields diagram (Fig. 2.2), and practically has analytical solutions for critical shear stress or sediment size.

CHAPTER 3

EVALUATION OF FACTORS OF SEDIMENT INCIPIENT MOTION

3.1 Introduction: Definition of Sediment Incipient Motion

Suppose there is a horizontal channel flow over a porous bed with uniform sediment particles (Fig. 3.1a). If all particles of the first layer are under incipient condition (general motion), a particle bears the following forces (Fig. 3.1b): (1) the submerged weight W ; (2) the hydrodynamic drag F_d and lift F_l ; (3) the cohesion F_c in both horizontal and vertical directions, which is a stretch force working like an adhesive tape; and (4) the friction F_f , and the bed support force F_n . Note that (1) the effect of hydrostatic pressure (or buoyancy) has been considered through the submerged weight W ; (2) the absolute hydrostatic pressure on fine particles (Xie 1980) is not considered in this research because even for fine sediment, there is always a porous bed flow; and (3) the first layer particles are loose in horizontal because of the water-bed interactions.

A sediment particle starts to move only if one of the following three conditions satisfies:

(1) If the driving moment with respect to point O [(Fig. 3.1(b)) due to F_d and F_l exceeds the restoring moment due to W and F_c , the particle starts to roll.

(2) If the drag F_d overcomes the resistance due to the friction F_f and the horizontal cohesion F_c , the particle starts to slide.

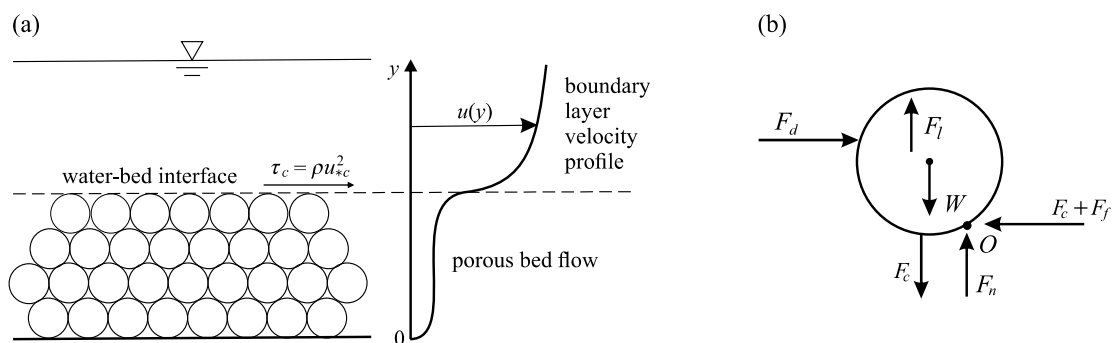


Figure 3.1: River flow with (a) velocity profile over a within porous bed; (b) forces on a bed particle

(3) If the lift F_l overcomes the submerged particle weight W and the vertical cohesion F_c , the particle starts to leap. Note that in this mode $F_n = 0$ but $F_c \neq 0$ because of cohesion.

These three modes make sediment incipient criterion nonunique. This explains why the data in the Shields diagram (Figs. 2.1 and 2.2) fall into a belt instead of a line. For simplicity, this research derives an incipient criterion based on the sliding mode, which requires [Fig. 3.1(b)]

$$F_d \geq F_c + F_f \quad (3.1)$$

Considering $F_d = (W - F_l) \tan \phi$ where ϕ = sediment friction angle, Eq. (3.1) becomes

$$F_d \geq F_c + (W - F_l) \tan \phi \quad (3.2)$$

Note that F_c in the vertical does not contribute to F_f because it acts only if a sediment

particle leaves bed.

Equation. (3.2) can be rearranged as

$$F_d + F_l \tan\phi \geq F_c + W \tan\phi \quad (3.3)$$

where the left-hand side can be combined as a resultant hydrodynamic force F_d including $F_l \tan\phi$. Therefore, Eq. (3.3) reduces to

$$F_d \geq F_c + W \tan\phi \quad (3.4)$$

which states that the key to finding the critical shear stress τ_c for sediment incipient motion is to accurately model the hydrodynamic force F_d and the cohesive force F_c , which are discussed below.

3.2 Hydrodynamic Force

The hydrodynamic force F_d in Eq. (3.4) includes the lift effect. This force is conventionally correlated to the near-bed boundary layer velocity profile [Fig. 3.1(a)] and the boundary friction factor. Yet, the current knowledge of boundary layer flow, such as Moody's diagram, cannot unify laminar and turbulent flows into a general law. Therefore, from the near-bed boundary layer flow theory; it is impossible to formulate a general sediment incipient equation that covers all the three regimes in Fig. 2.1 or the data in Fig. 2.2 for $0 \leq R_{*c} \leq \infty$

This research then considers sediment incipient motion a part of the porous bed flow [Fig. 3.1(a)], where the hydrodynamic drag is described by Forchheimer's law

(Guo and Zhang 2016):

$$F_d = \frac{C_d}{2} \rho V^2 \left(\frac{\pi D^2}{4} \right) \quad (3.5)$$

where V = bulk velocity through the first layer particles [Fig. 3(a)], and C_d = drag coefficient described by

$$C_d = \frac{A}{R} + B \quad (3.6)$$

where (A, B) = undetermined constants, and $R = \frac{VD}{\nu}$ is a Reynolds number. The first term on the right-hand side of Eq. (3.6) expresses the viscous effect, and the second term is the inertia effect.

At the water-bed interface [Fig. 3.1(a)], considering $V \propto u_{*c}$ and inserting Eq. (3.6)

into Eq. (3.5) results in

$$F_d = \left(\frac{A}{R_{*c}} + B \right) \left(\frac{1}{2} \rho u_{*c}^2 \right) \left(\frac{\pi D^2}{4} \right) \quad (3.7)$$

where (A, B) = new lumped parameters.

3.3 Cohesive Force

Except for the hydrodynamic force F_d , the cohesive force F_c is also required in Eq. (3.4). Referring to Fig. 3.2(a), a spherical sediment particle in water has a sediment core with diameter D and an attached water film with a thickness δ due to the molecular force between sediment and water. The attached water film serves as a surface glue to stick two or more sediment particles together. Strictly, the molecular force between a sediment core and its attached water is called the adhesive force (or adhesion); the molecular force between two sediment cores is called the cohesive

force. For simplicity, this research calls the resultant force as the cohesive force or cohesion.

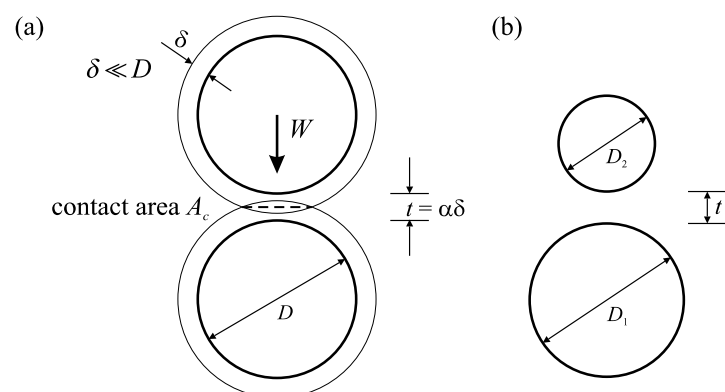


Figure 3.2: Cohesion between two sediment particles: (a) in water; (b) in air

Hamaker (1937) studied the cohesion between two particles in air [Fig. 3.2(b)]. He hypothesized that (1) each particle consists of many molecules; and the cohesive force is the sum of the molecular forces between two particles; and (2) the molecular force is described by the Van der Waals Force.

Based on these two hypotheses, Hamaker (1937) theoretically obtained the cohesive force F_c between two particles in air as:

$$F_c \propto \frac{1}{t^2} \frac{D_1 D_2}{D_1 + D_2} \quad (3.8)$$

where (D_1, D_2) = diameters of two particles, and t = distance between two particle surfaces [Fig. 4(b)] and $t \ll (D_1, D_2)$. For two identical particles, $D_1 = D_2 = D$, Eq. (3.8)

reduces to

$$F_c \propto \frac{D}{t^2} \quad (3.9)$$

which states that cohesion increases linearly with increasing particle diameter D , but quickly decreases as the separate distance t increases.

When applying Eq. (3.9) for study of sediment incipient motion, the effect of the attached water film must be considered. Several researchers (Xie 1980; Han and He 1999) then assumed

$$F_c = f(\delta, \text{water and sediment properties})D \quad (3.10)$$

where the function f reflects the effects of the attached water film and sediment-water properties. The thickness δ in all previous studies is assumed to be constant, which is not reasonable because as the water kinematic viscosity ν increases, δ should become thicker, and the attached water should become stickier.

Therefore, this research hypothesizes that: (1) The attached water film serves as a surface glue to stick two or more sediment particles together. Therefore, the adhesion between two sediment particles increases as the sticky water film thickness t [Fig. 3.2(a)] increases, i.e.,

$$F_c \propto t^m \propto (\alpha\delta)^m \quad (3.11)$$

where $t = \alpha\delta$, $1 \leq \alpha \leq 2$, and $m > 0$.

(2) The adhesion between two sediment particles is proportional to the contact area A_c [Fig. 4(a)]. This is derived from the experience of an adhesive tape for which adhesion is proportional to the contact area. For sediment with an attached water film, the contact area A_c [Fig. 3.2(a)] increases as the submerged sediment weight, $W = \left(\frac{\pi}{6}\right)(\gamma_s - \gamma)D^3$, increases. Therefore, it is assumed

$$F_c \propto A_c \propto \left(\frac{\pi}{6}\right)(\gamma_s - \gamma)D^3 \quad (3.12)$$

(3) The cohesion between two sediment particles due to electric charges is

described by Coulomb's law, inversely proportional to the square of distance between two particles. For two identical sediment particles, the distance between the two particle centers [Fig. 3.2(a)] is $D+t$ so that

$$F_c \propto \frac{1}{(D+t)^2} \approx \frac{1}{D(D+2t)} = \frac{1}{D(D+2\alpha\delta)} \quad (3.13)$$

where $t \ll D$ and the second order magnitude t^2 is negligible.

Combining Eqs. (3.11)-(3.12) results in

$$\frac{F_c}{\left(\frac{\pi}{6}\right)(\gamma_s - \gamma)D^3} = \frac{\alpha\delta^m}{D(D+2\alpha\delta)} \quad (3.14)$$

where the dimensional homogeneity requires $m=2$. Therefore, Eq (3.14) becomes

$$\frac{F_c}{\left(\frac{\pi}{6}\right)(\gamma_s - \gamma)D^3} = \frac{\alpha^2\delta^2}{D(D+2\alpha\delta)} = \frac{\alpha^2}{\left(\frac{D}{\delta}\right)\left(\frac{D}{\delta} + 2\alpha\right)} \quad (3.15)$$

which reduce to $F_c \propto D$ in Eq. (3.10) as $\delta \rightarrow 0$.

The thickness δ in Eq. (3.15) is still unknown. Because it increases as water kinematic viscosity ν increases. In still water, a dimensional analysis requires

$$\delta \propto \left[\frac{\nu^2}{(\Delta-1)g} \right]^{1/3} \quad (3.16)$$

where $\Delta = \rho_s/\rho$ is the specific gravity of sediment. Eq. (3.16) states that δ decreases as g increases, agreeing with the common understanding of the effect of gravity. In flowing water, except for Eq. (3.16), there is another viscous length scale, ν/u_{*c} , i.e.

$$\delta \propto \frac{\nu}{u_{*c}} \quad (3.17)$$

which implies that as the shear velocity u_{*c} (or the shear stress) on a sediment surface increases, the value of δ decreases.

Both length scales involve in sediment incipient motion because τ_{*c} can be written as

$$\tau_{*c} = \frac{R_{*c}^2}{D_*^3} \quad (3.18)$$

with

$$D_* = \left[\frac{(\Delta-1)g}{\nu^2} \right]^{1/3} D \quad (3.19)$$

where D is scaled by Eq. (3.16), and $D_* =$ dimensionless sediment diameter. Yet, in the critical particle Reynolds number R_{*c} in Eq.(3.18), D is scaled by Eq. (3.17). In flowing water, this research assumes that δ is dominated by Eq. (3.17) so that it is assumed

$$\delta = \beta \frac{\nu}{u_{*c}} \quad (3.20)$$

where $\beta =$ undetermined parameter.

Inserting Eq. (3.17) into Eq. (3.15) yields

$$\frac{F_c}{\left(\frac{\pi}{6}\right)(\gamma_s - \gamma)D^3} = \frac{\alpha^2}{\left(\frac{1Du_{*c}}{\beta\nu}\right)\left(\frac{1Du_{*c}}{\beta\nu} + 2\alpha\right)} = \frac{(\alpha\beta)^2}{R_{*c}(R_{*c} + 2\alpha\beta)} \quad (3.21)$$

which simplifies to

$$\frac{F_c}{\left(\frac{\pi}{6}\right)(\gamma_s - \gamma)D^3} = \frac{C}{R_{*c}(R_{*c} + 2\sqrt{C})} \quad (3.22)$$

where $C = (\alpha\beta)^2$. Mathematically, Eq. (3.22) states that as R_{*c} (or D) increases to infinity, the ratio of the cohesion to the gravity quickly decreases to zero; but as R_{*c} (or D) decreases to zero, the ratio tends to infinity. Physically, this implies that the cohesion is negligible for coarse sediment, but the gravity is negligible for fine sediment. These properties agree with the general understanding of the topic.

Eq. (3.22) with Eq. (3.7) is used below to find the critical shear stress for sediment incipient motion.

3.4 Critical Shear Stress

According to Eq. (3.4), the critical condition for sediment incipient motion is

$$F_d = F_c + W \tan \phi \quad (3.23)$$

Inserting Eqs. (3.7) and (3.22) into Eq. (3.23) results in

$$\left(\frac{A}{R_{*c}} + B\right) \left(\frac{1}{2} \rho u_{*c}^2\right) \left(\frac{\pi D^2}{4}\right) = \frac{C}{R_{*c}(R_{*c} + 2\sqrt{C})} \left(\frac{\pi}{6}\right) (\gamma_s - \gamma) D^3 + \left(\frac{\pi}{6}\right) (\gamma_s - \gamma) D^3 \tan \phi \quad (3.24)$$

which, divided by the friction term, is rearranged as

$$\frac{3}{4 \tan \phi} \left(\frac{A}{R_{*c}} + B\right) \frac{\rho u_{*c}^2}{(\gamma_s - \gamma) D^3} = \frac{C / \tan \phi}{R_{*c}(R_{*c} + 2\sqrt{C})} + 1 \quad (3.25)$$

Considering

$$\tau_{*c} = \frac{\rho u_{*c}^2}{(\gamma_s - \gamma) D} \quad (3.26)$$

and redefining the lumped constants as

$$\frac{3A}{4 \tan \phi} \rightarrow A, \frac{3B}{4 \tan \phi} \rightarrow B, \frac{C}{\tan \phi} \rightarrow C, 2\sqrt{C} \rightarrow E \quad (3.27)$$

Eq. (3.25) becomes

$$\left(\frac{A}{R_{*c}} + B\right) \tau_{*c} = \frac{C}{R_{*c}(R_{*c} + E)} + 1 \quad (3.28)$$

which gives

$$\tau_{*c} = \frac{\frac{C}{R_{*c}(R_{*c} + E)} + 1}{\frac{A}{R_{*c}} + B} \quad (3.29)$$

where the four lumped parameters (A, B, C, E) are determined by Eqs. (2.6)-(2.9).

First, Applying Eq. (2.7) in Eq. (3.29) results in $B=18$. Second, applying Eq. (2.6) gives $A=4C/E$. Eq. (3.29) then has only two parameters C and E , which are

determined by Eqs. (2.8) and (2.9), leading to $C=90$, $E=1$, and $A=360$. Therefore, Eq.

(3.29) is specified as

$$\tau_{*c} = \frac{\frac{90}{R_{*c}(R_{*c}+1)}+1}{\frac{360}{R_{*c}}+18} \quad (3.30)$$

This equation has clear physical meanings. The numerator expresses the resistance with the first term from the cohesion and the second term from the friction.

The denominator expresses the hydrodynamic driving force with the first term from the viscous drag and the second term from the inertia drag.

Eq. (3.30) simplifies to

$$\tau_{*c} = \frac{5}{19} \frac{1}{R_{*c}+1} - \frac{235}{171} \frac{1}{R_{*c}+20} + \frac{1}{18} \quad (3.31)$$

which is mathematically simpler than all pervious empirical equation (Jan 2018), and physically agrees with the data in Fig 2.2.

CHAPTER 4

APPLICATIONS

4.1 Introduction

Eq. (3.31) has two immediate applications: (1) Given a sediment diameter D , the critical shear stress τ_c can be solved analytically for sediment transport; and (2) given a bed shear stress τ_0 , the critical (minimum) sediment size D can be solved analytically for riprap design.

4.2 Critical shear stress for sediment transport

The critical shear stress τ_c (or τ_c^*) is required in many bedload transport equations (Chien and Wan 1999; Julien 2010; Jan 2018) and is governed by Eq. (3.31), which is solved analytically as follows:

First, applying Eq. (27) in Eq. (40) results in

$$\frac{R_{*c}^2}{D_*^3} = \frac{5}{19} \frac{1}{R_{*c}+1} - \frac{235}{171} \frac{1}{R_{*c}+20} + \frac{1}{18} \quad (4.1)$$

where τ_c involves only in R_{*c} . Eq. (4.1) can be rearranged as a quartic equation,

$$18R_{*c}^4 + 378R_{*c}^3 + (360 - D_*^3)R_{*c}^2 - D_*^3R_{*c} - 90D_*^3 = 0 \quad (4.2)$$

which has four roots mathematically (Fig. 4.1), but only one of them is physically true, which is

$$R_{*c} = \max(\text{real}([R_{*c1}, R_{*c2}])) \quad (4.3)$$

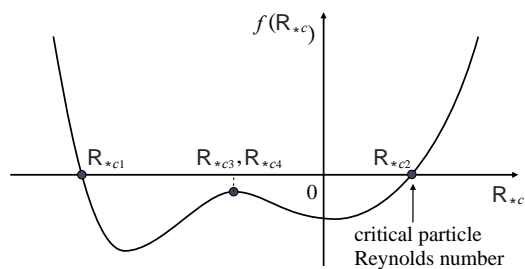


Figure 4.1: Graphical interpretation for solution of Eq. (4.2)

where

$$R_{*c1} = \sqrt{\frac{p}{2} \pm \frac{q}{4M} - M^2 - \frac{21}{4}} \pm M \quad (4.4)$$

$$p = \frac{D_*^3}{18} + \frac{1163}{8} \quad (4.5)$$

$$q = \frac{19D_*^3}{13} + \frac{7581}{8} \quad (4.6)$$

$$M = \frac{1}{2} \sqrt{\frac{2}{3}p + \frac{1}{3}\left(N + \frac{\Delta_0}{N}\right)} \quad (4.7)$$

$$N = \sqrt[3]{\frac{\Delta_1 + \sqrt{\Delta_1^2 - 4\Delta_0^3}}{2}} \quad (4.8)$$

$$\Delta_0 = \frac{1}{324}D_*^6 - \frac{1057}{18}D_*^3 + 400 \quad (4.9)$$

$$\Delta_1 = -\frac{1}{2916}D_*^9 - \frac{1087}{54}D_*^6 - \frac{156775}{3}D_*^3 + 16000 \quad (4.10)$$

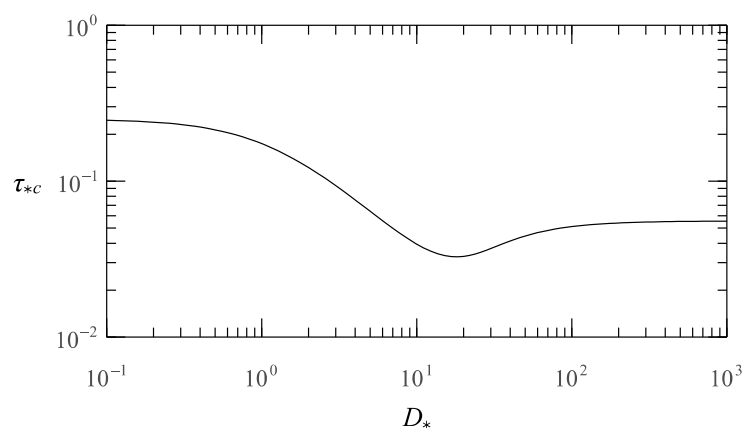


Figure 4.2 : Explicit Shields diagram in terms of $\tau_{*c} = f(D_*)$

Once R_{*c} is found, the critical Shields parameter τ_{*c} follows from Eq. 3.18).

Therefore, the explicit solution of the Shields diagram is found in terms of $\tau_{*c}=f(D_*)$,

shown in Fig. 4.2.

Practically, Eq. (4.3) can be replaced by mathematics software with

$$R_{*c} = \max(\text{real}([R_{*c1}, R_{*c2}, R_{*c3}, R_{*c4}])) \quad (4.11)$$

For example, using the Matlab function “roots.m”, R_{*c} is found with the following

sentences:

$$R_starc = \text{roots}([18, 378, 360-D_star.^3, -D_star.^3, -90*D_star.^3]);$$

$$R_starc = \max(\text{real}(R_starc));$$

Alternatively, R_{*c} is obtained from Eq. (4.1) by the following iterative equation:

$$R_{*c} = D_*^{3/2} \sqrt{\frac{5}{19} \frac{1}{R_{*c}+1} - \frac{235}{171} \frac{1}{R_{*c}+20} + \frac{1}{18}} \quad (4.12)$$

which converges rapidly with an initial guess, $R_{*c} = \sqrt{D_*^3/30}$, corresponding to

$$\tau_{*cmin} = 0.033.$$

Example Find the critical shear stress τ_{*c} for a sediment particle of $D=0.72\text{mm}$ with a kinematic water viscosity $\nu=10^{-6}\text{m}^2\text{s}^{-1}$. This example has

$$D_* = \left[\frac{(\Delta-10g)}{\nu^2} \right]^{1/3} D = \left[\frac{(2.65-(9.81))}{(10^{-6})^2} \right]^{1/3} (0.72*10^{-3})=18.213 \quad (4.13)$$

Eq. (4.3) results in $R_{*c}=14$, and Eq. (3.18) gives $\tau_{*c}=0.033$. The corresponding

dimensional critical shear stress is then $\tau_c =0.38\text{Pa}$.

4.3 Stable channel design

Riprap design of channel bed is to determine a minimum (critical) particle size that is unmovable, given a bed shear stress. This problem is also solved from Eq. (40), but

τ_{*c} needs to be rearranged as

$$\tau_{*c} = \frac{\tau_c}{(Y_s - Y)D} = \frac{u_{*c}^3}{(\Delta - 1)gv} \frac{v}{u_{*c}D} = \frac{x}{R_{*c}} \quad (4.14)$$

where

$$x = \frac{u_{*c}^3}{(\Delta - 1)gv} \quad (4.15)$$

is a dimensionless shear velocity parameter. Thus, Eq (3.31) becomes

$$\frac{x}{R_{*c}} = \frac{5}{19} \frac{1}{R_{*c} + 1} - \frac{235}{171} \frac{1}{R_{*c} + 20} + \frac{1}{18} \quad (4.16)$$

which can be rearranged as a cubic equation,

$$R_{*c}^2 + (1 - 18x)R_{*c}^2 + (90 - 378x)R_{*c} - 360x = 0 \quad (4.17)$$

which has three roots with the physical solution as:

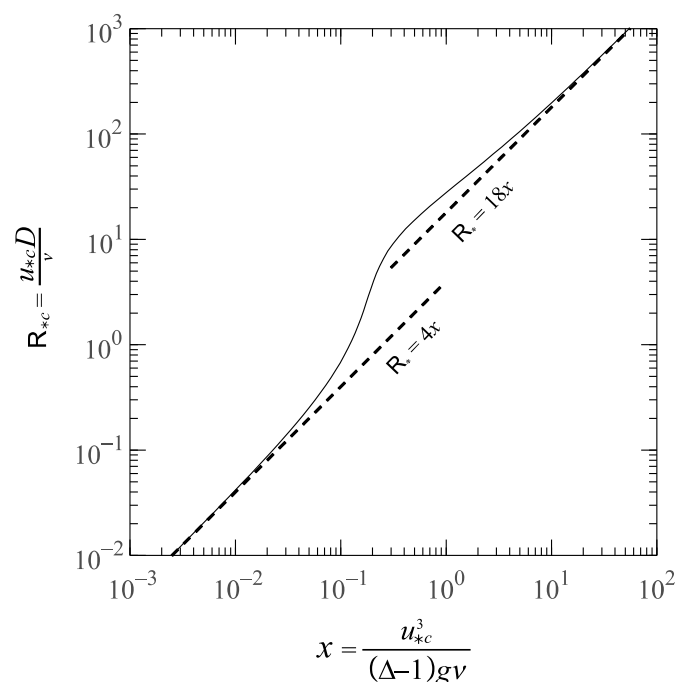


Figure 4.3: Analytical solution for riprap design from Eq. (58)

$$R_{*c} = 6x + \lambda - \frac{1}{3} + \frac{1}{\lambda} \left(36x^2 + 122x - \frac{269}{9} \right) \quad (4.18)$$

where

$$\lambda = \sqrt[3]{p + \sqrt{q}} \quad (4.19)$$

$$p = 216x^3 + 1098x^2 - 151x + \frac{404}{27} \quad (4.20)$$

$$q = -350892x^4 - 1353348x^3 + 1293777x^2 - \frac{994450}{3}x + 26925$$

(4.21)

Eq. (4.18) is the exact solution for riprap design in terms of $R_{*c} = f(x)$, shown in

Fig. 4.3 where the two asymptotes are: $R_{*c} = 18x$ as $x \rightarrow \infty$, and $R_{*c} = 4x$, as $x \rightarrow 0$.

Once R_{*c} is found, the particle size is determined by $D = vR_{*c}/u_{*c}$.

If the Matlab function “roots.m” is used, Eq.(4.17) is solved with the following

sentences:

```
R_starc = roots([1 1-18.*x 90-378.*x -360.*x]);
R_starc = max(real(R_starc));
```

Example A wide loose boundary channel with clear water has bottom slope

$S_0=0.001$ and flow depth $h=1\text{m}$, find the minimum sediment size D of the bed

material to maintain the channel stable?

The shear velocity of this channel is

$$u_{*c} = \sqrt{ghS_0} = \sqrt{(9.81)(1)(0.0001)} = 0.0313\text{ms}^{-1}$$

The x -value is then

$$x = \frac{u_{*c}^3}{(\Delta - 1)gv} = \frac{(3.1321 * 10^{-2})^3}{(2.65 - 1)(9.81)(10^{-6})} = 1.898$$

which, from Eq. (4.18), gives $R_{*c} = 46.87$. The minimum sediment size is thus

$$D = \frac{vR_{*c}}{u_{*c}} = \frac{(10^{-6})(46.87)}{0.0313} = 0.0015\text{m} = 1.5\text{mm}$$

CHAPTER 5

CONCLUSIONS AND RECOMMENDATIONS

5.1 Conclusions

This study revisited the classic problem of sediment initiation, presented a theoretical model for the Shields diagram, and obtained the following conclusions:

- 1) Sediment initiation has three modes; sliding, rolling, and leaping. Thus, a unique incipient criterion or a single incipient curve in the Shields diagram does not exist. The Shields diagram only represents an average incipient curve for sediment initiation.
- 2) It is impossible to generalize hydrodynamic drag on bed particles from channel boundary layer flow because of poor understanding of the water-bed interface flow. Yet, the drag can be expressed accurately by Forchheimer's law since flow through the first layer particles belongs to the porous bed flow.
- 3) Cohesion and adhesion are of importance for fine sediment particles. They are determined by attached water film and particle electrostatics. The water film serves as surface glue and functions like an adhesive tape; and the attractive force due to electronics follows Coulomb's law.
- 4) The Shields diagram can be theoretically derived as a rational function of the particle Reynolds number. It fits data well and tends to two constants for small

and large particle Reynolds numbers, respectively. It has a minimum value in the transitional regime.

- 5) The theoretical Shields diagram has two immediate applications: (1) Given a sediment size, the critical shear stress can be analytically solved in terms of dimensionless diameter for sediment transport; and (2) given a shear stress, the critical particle size can be analytically solved for riprap design. These applications are useful in river and coastal engineering, and sewer and drainage systems design.

5.2 Significance of model

The initiation of motion is involved in many geomorphic and hydraulic problems such as local scour, slope stability, stable channel design, etc. The Shields diagram empirically shows the dimensionless critical shear stress (i.e. the dimensionless shear stress required for the initiation of motion) is a function of a particular form of the particle Reynolds number, or Reynolds number related to the particle. This theoretical model would help us get better understanding on sediment initiation and transport. Sediment transport and initiation is applied to solve many environmental, geotechnical, and geological problems. Measuring or quantifying sediment transport and initiation or erosion is therefore important for coastal engineering. Sediment transport and initiation is important in the fields of

sedimentary geology, geomorphology, civil engineering and environmental engineering. Knowledge of sediment transport and initiation is most often used to determine whether erosion or deposition will occur, the magnitude of this erosion or deposition, and the time and distance over which it will occur.

5.3 Recommendations for future work

This research involved several hypotheses that have not tested directly with laboratory data and are recommended for future studies.

- (1) The Forcheimer equation is used to model the hydrodynamic force on a sediment particle. This equation was derived from flow within porous media. It is recommended to test its applicability by measuring drag on a sediment particle over a channel bed.
- (2) The cohesive force is assumed to be a combination of Hamaker's cohesive force in air and an analogy to cohesive tape. This hypothesis was not tested with direct data in this research. It should be carefully examined in future studies.

REFERENCES

- Ali, S. Z., and Dey, S. (2016). Hydrodynamics of sediment threshold. *Physics of Fluid*, 28, 075103
- Ali, S. Z., and Dey, S. (2017). Origin of the scaling laws of sediment transport. *Proc. Of the Royal Society A*, 473(2197), 1-19.
- Ali, S. Z., and Dey, S. (2018). Impact of phenomenological theory of turbulence of pragmatic approach to fluvial hydraulics. *Physics of fluids*, 30(4), 045105,1-11
- Armanini, A. (2005). Incipient sediment motion at high slopes in uniform flow condition. *Water Resources Research*, 41, W12431, doi:10.1029/2005WR004001.
- Bravo, R., Ortiz, P. and Pérez-Aparicio, J. L. (2014). Incipient sediment transport for non-cohesive landforms by the discrete element method (DEM). *Applied Mathematical Modelling*, 38(4), 1326-1337.
- Buffington, J. M. (1999). The legend of A. F. Shields. *J. Hydraulic Eng.*, 125(4), 376-387.
- Buffington, J. M., and Montgomery, D. R. (1997). A systematic analysis of eight decades of incipient motion studies, with special reference to gravel bedded rivers. *Water Resources Research*, 33(8), 1993-2029.
- Cao, Z., Pender G., and Meng, J. (2006). Explicit formulation of the Shields diagram for incipient motion of sediment. *J. Hydraulic Eng.*, 132(10), 1097-1099.
- Cheng, N. S., and Chiew, Y. M. (1999). Incipient sediment motion with upward seepage. *J. Hydraulic Res.* 37(5), 665-681.
- Chien, N., and Wan, Z. (1999). *Mechanics of Sediment Transport*. ASCE Press, Reston, VA.
- Dey, S. (1999). Sediment threshold. *Applied Mathematical Modelling*, 23(5), 399-417.
- Dey S. (2014). *Fluvial Hydrodynamics*. Springer, Berlin, Germany.
- Dey, S., and Ali, S.Z (2017). Stochastic mechanics of loose boundary particle transport in turbulent flow. *Physics of Fluid*, 29(5), 055103, 1-11

- Dey, S., and Ali, S. Z. (2017). Review article: Advances in modeling of bed particle entrainment sheared by turbulent flow. *Physics of Fluid*, 30(6), 061301, 1-30
- Du Boys, P. (1879). Le Rhône et les rivières a lit affouillable. Etude du régime du Rhône et de Faction exercée par les eaux sur un lit a fond de graviers indéfiniment affouillable. *Annales des Ponts et Chaussées*, 49(2), 141-195 (in French).
- Dou, G. (1960). Averaged velocity for sediment incipient motion. *J. Hydraulic Eng.*, 5(4), 44-60 (in Chinese).
- Dou, G. (1999). Further study on sediment incipient velocity. *J. Hydraulic Eng.*, 16(9), 1-9 (in Chinese).
- Ettema, R. (2006). Hunter Rouse - His work in retrospect. *J. Hydraulic Eng.*, 132 (12): 1248-1258.
- Fredsoe, J., and Deigaard, R. (1992). *Mechanics of Coastal Sediment Transport*. World Scientific, Singapore.
- Garcia, M. (2008). *Sedimentation Engineering*. ASCE Press, Reston, VA.
- Guo, J. (2002). Hunter Rouse and Shields Diagram. *Advances in Hydraulics and Water Engineering - Proceedings of the 13th IAHR-APD Congress, Singapore, 6-8 August 2002*. 2. World Scientific. pp. 1096-1098.
- Guo, J., and Zhang, J. (2016). Velocity distributions in laminar and turbulent vegetated flows. *J. Hydraulic Res.*, 54(2), 117-130.
- Hager, W. H. (2005). Du Boys and sediment transport. *J. Hydraulic Res.*, 43(3), 227-233.
- Hamaker, H. C. (1937). The London-Van der Waals attraction between spherical particles. *Physica IV*, 4(10), 1058-1072.
- Han, Q.-W., and He, M.-M. (1999). *Laws of Sediment Threshold and Critical Velocity*. Science Press, Beijing, China (in Chinese).
- Ikeda, S. (1982). Incipient motion of sand particles on side slopes. *J. Hydraulic Eng.*, 108(1), 95-114.

- Iwagaki, Y. (1965). Fundamental study on critical tractive force. Transactions of Japanese Society of Civil Engineers, 41(1),1-21.
- Jan, C. D. (2018). *Mechanics of Sediment Transport*. Wu-Nan Book Inc., Taiwan, China (in Chinese).
- Julien, P. Y. (2010). *Erosion and Sedimentation*. 2nd ed. Cambridge University Press, New York.
- Kennedy, J. F. (1995). The Albert Shields Story. *J. Hydraulic Eng.*, 121(11), 766-772.
- Lamb, M. P., Dietrich, W. E., and Venditti, J. G. (2008). Is the critical Shields stress for incipient sediment motion dependent on channel-bed slope? *J. Geophysical Res.*, 113, F02008, doi:10.1029/2007JF000831.
- Li, S., Lu, Y., Zuo, L., Huang, W., and Lu, Y. (2013) Incipient sediment motion in steady boundary layers. *Advances in Water Science*. 24(6), 821-829 (in Chinese).
- Mants, P. A. (1977). Incipient transport of fine grains and flakes by fluids -- Extended Shields diagram. *J. Hydraulic Eng.*, 103(6), 601-615.
- Marion A., Tregnaghi M. (2013) A New Theoretical Framework to Model Incipient Motion of Sediment Grains and Implications for the Use of Modern Experimental Techniques. In: Rowiński P. (eds) *Experimental and Computational Solutions of Hydraulic Problems*. GeoPlanet: Earth and Planetary Sciences. Springer, Berlin, Heidelberg
- Miedema, S. A. (2010). Constructing the Shields curve, a new theoretical approach and its applications. *Proc. WODCON XIX*, Beijing China.
- Righetti, M., and Lucarelli, C. (2007). May the Shields theory be extended to cohesive and adhesive benthic sediments? *J. Geophys. Res.* 112, C05039, Doi: 10.1029/2006JC003669
- Roarty, H. J., and Bruno, M. S. (2006). Laboratory measurements of bed load sediment transport dynamics. *J. Waterway, Port, Coastal, and Ocean Engineering*, 132(3), 199-211.
- Roušar, L., Zchoval, Z., and Julien, P. (2016). Incipient motion of coarse uniform gravel. *J. Hydraulic Res.*, 54(6), 615-630.

- Rouse, H. (1939). *An analysis of sediment transportation in the light of fluid turbulence*. USDA Soil Cons. Service SCS-TR 25, Washington D.C.
- She, K., Trim, L., and Pope, D. J. (2014). Threshold of motion of natural sediment particles in oscillatory flows. *J. Coastal Res.*, 22(3), 701-709.
- Shields, A. (1936). *Application of similarity principles and turbulence research to bed-load movement*. Hydrodynamics Laboratory Publ. No. 167, W. P. Ott, and J. C. van Uchelen, trans., U.S. Dept. of Agr., Soil Conservation Service Cooperative Laboratory, California Institute of Technology, Pasadena, CA.
- Simoës, F. J. M. (2014). Shear velocity criterion for incipient motion of sediment. *Water Science and Eng.*, 2014, 7(2): 183-193.
- Sun, Z., Xie, J., and Xie B. (1997). Incipient motion of Individual fractions of nonuniform sediment. *J. Hydraulic Eng.* 28(10), 25-32 (in Chinese).
- Tang, C. (1963), Averaged velocity for sediment incipient motion. *J. Hydraulic Eng.* 7(2), 1-12 (in Chinese).
- Xie, J.-H. (1980). *River Sedimentation Engineering*. Water Resources Press, Beijing, China (in Chinese).
- Yalin, M. S., and Karahan, E. (1979). Inception of sediment transport. *J. Hydraulic Eng.*, 105(11), 1433-1443.
- You, Z.-J (1998). Initial motion of sediment in oscillatory flow. *J. Waterway, Port, Coastal, and Ocean Eng.*, 124(2), 68-72.
- You, Z.-J., and Yin, B. (2006)). A unified criterion of sediment motion and inception of sheet flow under water waves. *Sedimentology.*, 53(5), 1181-1190.
- Zhang, R., Xie, J., and Chen, W. (1961). *River Dynamics*. China Industry Press, Beijing, China (in Chinese).

Appendix I

Generalization of Shields Diagram

When the Shields diagram is extended to bottom wave boundary lay flow, because water oscillations increase sediment mobility, the dimensionless critical shear stress τ_{*c} for large particle Reynolds number, $R_{*c} \rightarrow \infty$, is measured to be 0.045 (You 1998; and Yin 2006) instead of 0.056, In such a case, the four model parameter in Eq. (3.30) are determined as follows:

Referring to Fig. 5.1, supposed the four restriction conditions are

$$\tau_{*c}(R_{*c} \rightarrow 0) = \tau_{*c0} \quad (1)$$

$$\tau_{*c}(R_{*c} \rightarrow \infty) = \tau_{*c\infty} \quad (2)$$

$$\tau_{*c}(R_{*c} = R_{*cmin}) = \tau_{*cmin} \quad (3)$$

$$\frac{d\tau_{*c}}{dR_{*c}}(R_{*c} = R_{*cmin}) = 0 \quad (4)$$

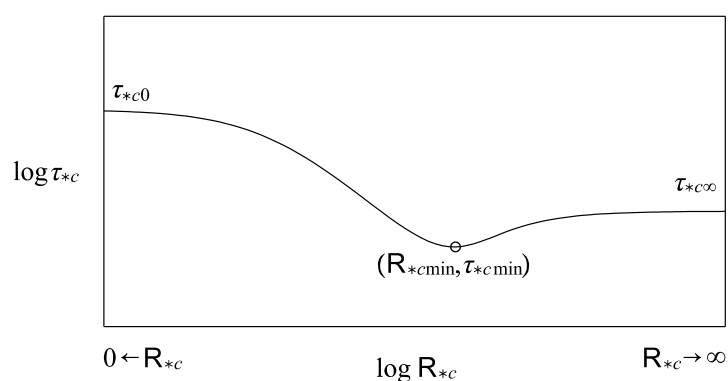


Figure 5.1: Generalization of Shields diagram

First, applying Eq. (1) in Eq. (3.30) gives

$$B = \frac{1}{\tau_{*\infty}} \quad (5)$$

Second, applying Eq. (3) in Eq. (39) gives

$$A = \frac{C}{\tau_{*c0}E} \quad (6)$$

Third, Eq, (3.30) gives

$$\frac{\frac{C}{(R_{*min}(R_{*min}+E)+1)}+1}{\frac{1}{R_{*min}\tau_{*c0}}+\frac{1}{\tau_{*c\infty}}} = \tau_{*cmin} \quad (7)$$

Eq. (4) results in

$$\frac{\frac{C}{E}+\frac{\tau_{*\infty}^2}{\tau_{*c0}}+(\tau_{*c0}-\tau_{*c\infty})E}{(R_{*min}+\frac{C\tau_{*\infty}^2}{E\tau_{*c0}})^2} = \frac{\tau_{*c0}E}{(R_{*min}+E)^2} \quad (8)$$

Solving Eqs. (7) and (8) simultaneously for C and E results in

$$\frac{E}{R_{*c}} = \left(1 - \frac{\tau_{*cmin}}{\tau_{*c0}}\right)^{-1/2} - 1 \quad (9)$$

$$\frac{C}{R_{*min}E} = \left(1 - \frac{\tau_{*cmin}}{\tau_{*c\infty}}\right)\left(\frac{\tau_{*cmin}}{\tau_{*c0}} - \frac{1}{1+\frac{R_{*min}}{E}}\right)^{-1} \quad (10)$$

Once C and E are found from Eqs. (9) and (10) , A follows from Eq. (6).